

RESEARCH MEMORANDUM

EXPERIMENTAL STUDY OF THE EFFECTS OF SCALE ON THE
ABSOLUTE VALUES OF ZERO-LIFT DRAG OF AIRCRAFT
CONFIGURATIONS AT TRANSONIC SPEEDS

By Robert R. Howell and Albert L. Braslow

Langley Aeronautical Laboratory
Langley Field, Va.

NATIONAL ADVISORY COMMITTEE
FOR AERONAUTICS

WASHINGTON

February 8, 1957

Declassified January 12, 1961

NATIONAL ADVISORY COMMITTEE FOR AERONAUTICS

RESEARCH MEMORANDUM

EXPERIMENTAL STUDY OF THE EFFECTS OF SCALE ON THE
ABSOLUTE VALUES OF ZERO-LIFT DRAG OF AIRCRAFT
CONFIGURATIONS AT TRANSONIC SPEEDS

By Robert R. Howell and Albert L. Braslow

SUMMARY

An investigation has been made at Mach numbers from 0.7 to 1.4 to determine the effects of scale on the zero-lift drag of a fin-stabilized body of revolution and a fighter-type airplane configuration. Results obtained at relatively low values of the Reynolds number in the Langley transonic blowdown tunnel were compared with larger scale data obtained on geometrically similar models in free flight.

Absolute values of the zero-lift drag coefficient measured in the wind tunnel agreed closely with the free-flight values through the test Mach number range after adjustments were made for the effect on viscous drag of differences in Reynolds number between the two test conditions. The pressure-drag variation with Mach number was found to be independent of the Reynolds number adjustment to the skin friction. The experimentally determined values of subsonic drag coefficient for the complete airplane configuration were approximately 0.005 greater than the value estimated on the basis of turbulent skin friction and equivalent flat-plate wetted area largely as a result of pressure drag associated with local flow conditions.

INTRODUCTION

An accurate estimation of the absolute drag coefficient of a complete airplane configuration through the transonic speed range is difficult to make. Prediction of the transonic drag rise, which is the most difficult phase of the estimation, is usually accomplished with the use of the methods of references 1 and 2. These theoretical predictions of the drag rise have been found to vary significantly in accuracy with changes in the complexity of the configuration. In fact, differences between the computed drag rise and experimentally determined values

have been as large as 26 percent (ref. 1). Inasmuch as theoretical prediction of the drag curve is not as reliable as may be desired even after an appreciable expenditure of manpower and time, other possible solutions to the problem should be considered.

One such possibility is the experimental determination of the drag variation with Mach number of a small-scale model of the configuration in a small transonic wind tunnel. A question raised by this approach is whether drag data so obtained at relatively low values of the Reynolds number can be correctly interpreted in terms of flight conditions. Accordingly, an investigation was made at transonic speeds of scale effects on the zero-lift drag of a fin-stabilized body of revolution and a typical fighter-type airplane configuration having air inlets with internal air flow. The small-scale wind-tunnel tests were made in the Langley transonic blowdown tunnel and larger scale results used for comparison were obtained in free flight by the Langley Pilotless Aircraft Research Division.

SYMBOLS

A area

C_{DT} total drag coefficient, $\frac{\text{Measured drag}}{q_0 S}$

C_{Db} base drag coefficient, $-\frac{(p_b - p_o) A_b}{q_0 S}$

C_{Di} internal drag coefficient, $\frac{m(v_o - v_e)}{q_0 S} - \frac{(p_e - p_o) A_e}{q_0 S}$

C_D net drag coefficient, $C_{DT} - C_{Db}$ for body of revolution
or $C_{DT} - C_{Di} - C_{Db}$ for the airplane configuration

ΔC_D pressure-drag coefficient rise, $C_D - C_{D_{M_o=.9}}$

ΔC_{Df} increment in pressure-drag coefficient rise due to the fins,
 $(C_D - C_{D_{M_o=.9}})_{\text{fins on}} - (C_D - C_{D_{M_o=.9}})_{\text{fins off}}$

\bar{c} mean aerodynamic chord of wing

S	reference area; maximum body frontal area for the body of revolution (0.511 sq in.) or wing plan-form area for the airplane configuration (13 sq in.)
L	total length of the body of revolution
m	local mass flow, ρVA
$\frac{m_i}{m_o}$	mean inlet mass-flow ratio, $\frac{m_i}{\rho_o V_o A_i}$
M	Mach number
p	static pressure
q	dynamic pressure, $0.7\rho M^2$
V	velocity
r	body radius
ρ	mass density
R	Reynolds number based on length of body of revolution or on wing mean aerodynamic chord of airplane model
x	body longitudinal station

Subscripts:

b	base
i	inlet
e	exit
o	free stream
max	maximum

MODELS, APPARATUS, AND TESTS

Models

Fin-stabilized body.- The body shape tested is defined by the equation

$$r = r_{\max} - a(0.6L - x)^2$$

where

$$a = 0.01097 \text{ per in.} \quad (0 < x < 0.6L)$$

$$a = 0.01445 \text{ per in.} \quad (0.6L < x < L)$$

A sketch of the body tested is presented as figure 1 where the pertinent model body and fin dimensions are shown. A photograph of the model is presented as figure 2. All of the dimensions used in constructing the model were scaled down values of those presented in reference 3 which contains a description of the model used for the free-flight tests. The overall fineness ratio of the body was 12.5.

The initial model was constructed of a polyester resin strengthened with glass fibers. The fins were lost, however, during the initial test presumably because of flutter, and, subsequently, were reconstructed of a stiffer plastic material.

Airplane model.- The airplane model tested was a $\frac{1}{52.6}$ -scale model of a version of a specific airplane, a configuration which would provide a critical test of the construction problems involved. The ordinates used to design the external shape of the model were scaled down from values measured on a larger model of the same airplane which was tested in free flight at zero lift by the Langley Pilotless Aircraft Research Division. A line drawing of the configuration is presented in figure 3, and the general dimensions are given in table 1. A tail inclination of -0.63° was selected for the airplane model, which had a cambered wing leading edge, in order to provide zero pitching moment at zero lift.

The internal ducts aft of the twin air scoops were merged to a common duct of annular cross section which exited at the base of the model. The minimum duct area, which was located at the base of the model, amounted to 86.2 percent of the total inlet area.

The model was constructed of plastic cast around steel inserts in the wing and tail and with steel ducting and balance shield to provide

the required stiffness and strength to avoid aeroelastic deflection and flutter. Female templates which were jig located longitudinally were used to check the fuselage contour. Airfoil templates at four spanwise stations were used to insure that the wing was properly contoured. Photographs of the airplane model are presented as figure 4. It may be of interest to note that this model of a complete airplane configuration was constructed with an expenditure of less than 500 man hours of labor.

Apparatus

Both the body of revolution and the airplane model were mounted to single-component internal strain-gage balances which were sting supported in the wind tunnel (figs. 1 and 3). The body of revolution was set at zero angle of attack by use of a sensitive inclinometer. The airplane model was set at close to zero lift by adjusting the angle of attack until zero longitudinal aerodynamic moment was recorded by a strain gage attached to the sting some distance behind the model.

The base pressures for both models were measured by inserting an open-end tube through the center of the sting into an open section of the balance. In the case of the airplane configuration, a total-pressure rake consisting of six total-pressure tubes (fig. 5) was used to measure the total pressure of the internal flow as it exited from the model. The average of these total pressures in conjunction with the measured static pressure was used to determine the inlet mass-flow ratio and the drag due to the internal flow at subsonic speeds. At supersonic speeds, the exit was choked, and the measured total pressures determined the static pressure that was used in the calculations.

All of the measured pressure data were recorded on quick-response flight-type pressure recorders. The drag force measurements were recorded as time histories by pen-type self-balancing potentiometers.

Tests

The tests were made in the Langley transonic blowdown tunnel. This tunnel has a slotted test section of octagonal cross section with 26 inches between flats. Previous experience in testing models of the same size in this wind tunnel has indicated that the model drag forces are affected by the intersection of wall-reflected model disturbances with the model in the Mach number range between about 1.04 and 1.13. Therefore, no drag data are presented for this Mach number range.

In order to avoid the effect on drag due to a possible variation in location of the boundary-layer transition point, both of the models were tested with transition fixed by roughness strips. These strips were

constructed by blowing 0.001- to 0.002-inch-diameter carborundum particles on a strip of wet shellac. Reference 4 provides a guide to the minimum size of such three-dimensional type of roughness required to cause transition from laminar flow to turbulent flow. For the body of revolution, a 1/4-inch-wide roughness band was placed around the model 1 inch behind the nose of the body. Tests were also made with this model smooth to determine the effect of roughness on the drag level of the body. For the airplane model, 1/8-inch-wide roughness strips were placed on both wing surfaces 10 percent of the local chord behind the wing leading edge. There was also a 1/8-inch-wide band around the nose of the fuselage and located 1/2 inch behind the nose boom-fuselage intersection (fig. 3). No roughness strips were applied to the tail surfaces of either model. Inasmuch as the wetted area of the tail surfaces influenced by possible changes in extent of laminar flow was small compared with the total wetted area of the entire configuration, differences in the extent of laminar flow on the tails would cause no significant change in the viscous drag of the models.

The major portion of the tests of the fin-body combination was run at a reduced stagnation pressure of 25 lb/sq in. abs in an effort to avoid excessive fin loads and thereby insure retainment of the fins for the duration of the tests. After testing was completed at a stagnation pressure of 25 lb/sq in. abs, some additional check test points were obtained at a stagnation pressure of 50 lb/sq in. abs. This higher stagnation pressure afforded better accuracy and a higher ultimate test Mach number. All the tests of the body without fins were made at a stagnation pressure of 50 lb/sq in. abs. The tests of the airplane configuration were made entirely at a stagnation pressure of 25 lb/sq in. abs as a result of the stress limitations of the balance used.

The Reynolds number variation was between about 0.67×10^6 and 0.75×10^6 per inch for the tests at a stagnation pressure of 25 lb/sq in. abs and between about 1.3×10^6 and 1.4×10^6 per inch for the tests at a stagnation pressure of 50 lb/sq in. abs. (See fig. 6 for Reynolds numbers based on reference lengths.) The corresponding Mach number ranges were between 0.70 and 1.24 for the stagnation pressure of 25 lb/sq in. abs and between 0.8 and 1.4 for the stagnation pressure of 50 lb/sq in. abs.

The drag data measured at Mach numbers greater than about 1.15 were corrected for buoyancy effects resulting from the longitudinal gradients in test section Mach number. This buoyancy correction was based on the model volume and the Mach number gradients measured in the test section with no model present.

The estimated maximum overall error in the faired curves for the indicated parameters are presented in the following table:

C_D for -	
Body of revolution	± 0.010
Airplane configuration	± 0.0010
M_0	± 0.01
C_{D_i}	± 0.0005
C_{D_b} for -	
Body of revolution	± 0.005
Airplane configuration	± 0.0005
m_i/m_0	± 0.01

RESULTS AND DISCUSSION

Fin-Stabilized Body

The drag data for the fin-stabilized body of revolution are presented in coefficient form in figure 7. Presented are total drag coefficient, base drag coefficient, and net drag coefficient as a function of the Mach number. The differences in drag coefficient due to placing the roughness band around the nose of the wind-tunnel model were small and generally within the scatter of test data; thus, little, if any, laminar flow existed on the supposedly "smooth" model and the drag increment due to the roughness particles themselves was within experimental accuracy. From the results presented in reference 4, it appears that, for the present tests, extreme care would have been required to obtain model surfaces sufficiently smooth to obtain any laminar flow. In fact, reference 4 indicates that three-dimensional roughness particles as small as approximately 0.0005 inch would have been large enough to cause premature transition from laminar flow to turbulent flow at even the lowest test Reynolds number.

For comparative purposes, the corresponding drag coefficients as obtained from free-flight tests (refs. 3 and 5) are also presented in figure 7. It should be pointed out that the free-flight base drag coefficients presented are not those actually measured on the present body shape. A comparison of base pressures measured on the present body shape in free flight with other free-flight base-pressure measurements indicated that the present free-flight results were in error, probably because of the effect on the base-pressure measurements of an unintentional burning of a residue of rocket propellant. Hence, the base pressure drag obtained from base pressures measured in free flight on another body having an identical afterbody and fin and a different nose but with no apparent rocket propellant residue in the model (ref. 5) has been used in the

present analysis. The difference in base-drag measurements indicated in figure 7 between the wind-tunnel and free-flight tests is believed to be due primarily to the effect on the wind-tunnel results of the presence of the model support sting. This difference is not considered important, however, since its magnitude is generally small enough to be well within the combined accuracy of the two sets of measured results.

Presented in figure 8 is a comparison of the variation of the pressure-drag-coefficient increment with Mach number as obtained from the two test techniques at widely different values of Reynolds number - 30×10^6 to 70×10^6 for the free-flight tests as compared with 6.8×10^6 to 7.6×10^6 for the wind-tunnel tests (fig. 6). This increment, as presented, is the drag-coefficient increase at Mach numbers greater than 0.9. As can be seen, the measured drag rise was independent of the value of Reynolds number and indicated that any differences in pressure drag associated with local separation effects were of negligible importance.

The faired net drag coefficients of the fin-body combination as obtained from the basic data results of the two test techniques are replotted in figure 9. This figure indicates a large difference in the absolute level of the drag coefficient throughout the Mach number range, although the drag rise measurements agreed very well as previously indicated in figure 8. Inasmuch as the flight Reynolds numbers were large enough to result in turbulent boundary-layer flow over the major part of the configuration and the transition strips insured turbulent flow over the wind-tunnel model, the difference in drag coefficient is attributed to the difference in turbulent skin friction between the two tests. The wind-tunnel results, therefore, were adjusted by decreasing the drag coefficients an amount equivalent to the decrease in turbulent skin-friction coefficient of the component parts of the configuration (body and fins) resulting from an increase in Reynolds number from the tunnel to flight values. The turbulent skin-friction data of reference 6 were used for this adjustment at each Mach number. As indicated in figure 9, the absolute values of the wind-tunnel drag coefficients adjusted to the free-flight Reynolds numbers agree very well with the free-flight measurements. The estimate of skin-friction drag coefficient at $M = 0.8$ shown in figure 9 was computed on the basis of turbulent flow and equivalent flat-plate wetted area at free-flight Reynolds number. It is indicated that, for a smoothly contoured configuration of this type, such an estimate provides an accurate indication of the subsonic drag coefficient level.

A further indication of the correctness of the measured absolute level of the wind-tunnel drag results and thereby the correctness of the Reynolds number adjustment can be obtained from a comparison of the total drag characteristics of the wind-tunnel model with those of a very similar configuration tested in free flight at Reynolds numbers about equal to the wind-tunnel values (fig. 10). This free-flight model (ref. 7) differed from the present configuration by only a negligible difference

in forebody fineness ratio. The nose fineness ratio was 7.50 for the wind-tunnel model and 7.13 for the free-flight model. No base pressures were measured on this free-flight model; hence, the comparison of results from the two test techniques can be made on the basis of total drag coefficient only. Based on the previous comparison of base drag coefficients (fig. 7), however, it would appear that the base-pressure differences could be neglected for the present afterbody shape and thereby justify for this case the direct comparison of total drag coefficients. It should be mentioned that the surface condition of the free-flight model was such that any difference in drag coefficient due to possible laminar flow is believed to be negligible. The comparison presented in figure 10 substantiates the previous results in that, if Reynolds number effects are accounted for, agreement is obtained not only in the values of pressure-drag coefficient rise but also in the absolute values of drag coefficient.

An added point of interest obtained from the tests of the fin-stabilized body of revolution is an evaluation of the effect of the fins on the pressure drag. The increment in pressure-drag coefficient due to the presence of the fins ΔC_{D_f} is presented in figure 11 as a function of Mach number. Presented for comparison are some unpublished results as obtained in free flight by a somewhat different technique. This technique involved measurement of the drag of fin-stabilized cone-cylinder combinations and calculations of the pressure drag associated with the cone. Excellent agreement was obtained except in the speed range near Mach number 1.0 where some small differences in fin pressure drags are indicated.

Airplane Model

The results of the investigation of the $\frac{1}{52.6}$ -scale airplane model are presented in coefficient form as a function of Mach number in figure 12. The faired net-drag-coefficient curve is reproduced in figure 13 for comparative purposes. The wind-tunnel data have been adjusted as previously described for Reynolds number effects to correspond to the free-flight data, which are also presented in the same figure.

The agreement in the values of absolute drag coefficient as well as the magnitude of pressure-drag rise is considered to be very good; however, two possible factors other than the experimental accuracy of each individual test may underlie the indicated small difference ($\Delta C_D = 0.0020$) in pressure-drag rise between the wind-tunnel and the free-flight results. One is the fact that the free-flight tests were made at an air-inlet mass-flow ratio of approximately 0.8 whereas the wind-tunnel tests were made at a mass-flow ratio of 0.7 or less. The other factor is a possible subsonic drag difference due to the increase in model afterbody pressures resulting from the presence of the model support sting in the case of the wind-tunnel tests (ref. 8).

An estimate of skin-friction drag coefficient at $M = 0.8$ similar to that made for the fin-stabilized body of revolution is also shown in figure 13. Although the effect of induced velocities on the skin friction has not been included in this estimate, calculations indicated that the increment in skin-friction drag due to these induced velocities would be only a small part of the indicated difference between the subsonic drag level determined experimentally and that estimated on the basis of equivalent flat-plate wetted area. The larger part of this indicated difference most probably results from pressure drag associated with the air inlets, the boundary-layer bypass, and flow interference in the region of the wing-root juncture and near the empennage (ref. 9). This type of pressure drag cannot be handled analytically and, therefore, computations of the absolute subsonic drag coefficient level of such complex airplane configurations may be unreliable.

CONCLUDING REMARKS

An investigation has been made at Mach numbers from 0.7 to 1.4 of the effects of scale on the zero-lift drag of a fin-stabilized body of revolution and a fighter-type airplane configuration. Results obtained at relatively low values of the Reynolds number in the Langley transonic blowdown tunnel were compared with larger scale data obtained on geometrically similar models in free flight.

Absolute values of the zero-lift drag coefficient measured in the wind tunnel agreed closely with the free-flight values through the test Mach number range after adjustments were made for the effects on viscous drag of differences in Reynolds number between the two test conditions. The pressure-drag variation with Mach number was found to be independent of the Reynolds number adjustment to the skin friction. The experimentally determined values of subsonic drag coefficient for the complete airplane configuration were approximately 0.005 greater than the value estimated on the basis of turbulent skin friction and equivalent flat-plate wetted area largely as a result of pressure drag associated with local flow conditions.

Langley Aeronautical Laboratory,
National Advisory Committee for Aeronautics,
Langley Field, Va., October 12, 1956.

REFERENCES

1. Holdaway, George H.: Comparison of Theoretical and Experimental Zero-Lift Drag-Rise Characteristics of Wing-Body-Tail Combinations Near the Speed of Sound. NACA RM A53H17, 1953.
2. Holdaway, George H., and Mersman, William A.: Application of Tchebichef Form of Harmonic Analysis to the Calculation of Zero-Lift Wave Drag of Wing-Body-Tail Combinations. NACA RM A55J28, 1956.
3. Hart, Roger G., and Katz, Ellis R.: Flight Investigations at High-Subsonic, Transonic, and Supersonic Speeds To Determine Zero-Lift Drag of Fin-Stabilized Bodies of Revolution Having Fineness Ratios of 12.5, 8.91, and 6.04 and Varying Positions of Maximum Diameter. NACA RM L9I30, 1949.
4. Von Doenhoff, Albert E., and Horton, Elmer A.: A Low-Speed Experimental Investigation of the Effect of a Sandpaper Type of Roughness on Boundary-Layer Transition. NACA TN 3858, 1956.
5. Katz, Ellis, and Stoney, William E., Jr.: Base Pressures Measured on Several Parabolic-Arc Bodies of Revolution in Free Flight at Mach Numbers From 0.8 to 1.4 and at Large Reynolds Numbers. NACA RM L51F29, 1951.
6. Rubesin, Morris W., Maydew, Randall C., and Varga, Steven A.: An Analytical and Experimental Investigation of the Skin Friction of the Turbulent Boundary Layer on a Flat Plate at Supersonic Speeds. NACA TN 2305, 1951.
7. Stoney, William E., Jr.: Some Experimental Effects of Afterbody Shape on the Zero-Lift Drag of Bodies for Mach Numbers Between 0.8 and 1.3. NACA RM L53I01, 1953.
8. Cahn, Maurice S.: An Experimental Investigation of Sting-Support Effects on Drag and a Comparison With Jet Effects at Transonic Speeds. NACA RM L56F18a, 1956.
9. Howell, Robert R.: An Experimental Study of the Zero-Angle-of-Attack Transonic Drag Associated With the Vertical Position of a Horizontal Tail at Zero Incidence. NACA RM L56H07, 1956.

TABLE I

AIRPLANE-MODEL GEOMETRIC CHARACTERISTICS

Wing:

Airfoil section at root (free-stream)	NACA 65A006 (mod.)
Airfoil section at tip (free-stream)	NACA 65A004 (mod.)
Area (included), sq in.	13.27
Aspect ratio	3.92
Taper ratio	0.49
Sweepback (quarter chord), deg	35
Incidence, deg	0
Dihedral, deg	-2.50

Horizontal tail:

Airfoil section at root (free-stream)	NACA 65A006
Airfoil section at tip (free-stream)	NACA 65A004
Area (included), sq in.	3.57
Aspect ratio	3.65
Taper ratio	0.40
Sweepback (quarter chord), deg	35
Incidence, deg	-0.63
Dihedral, deg	0

Vertical tail:

Airfoil section (free-stream)	NACA 0006
Area, sq in.	2.10
Aspect ratio	3.02
Taper ratio	0.18

Duct areas:

Duct inlet, sq in.	0.1658
Duct exit, sq in.	0.1425

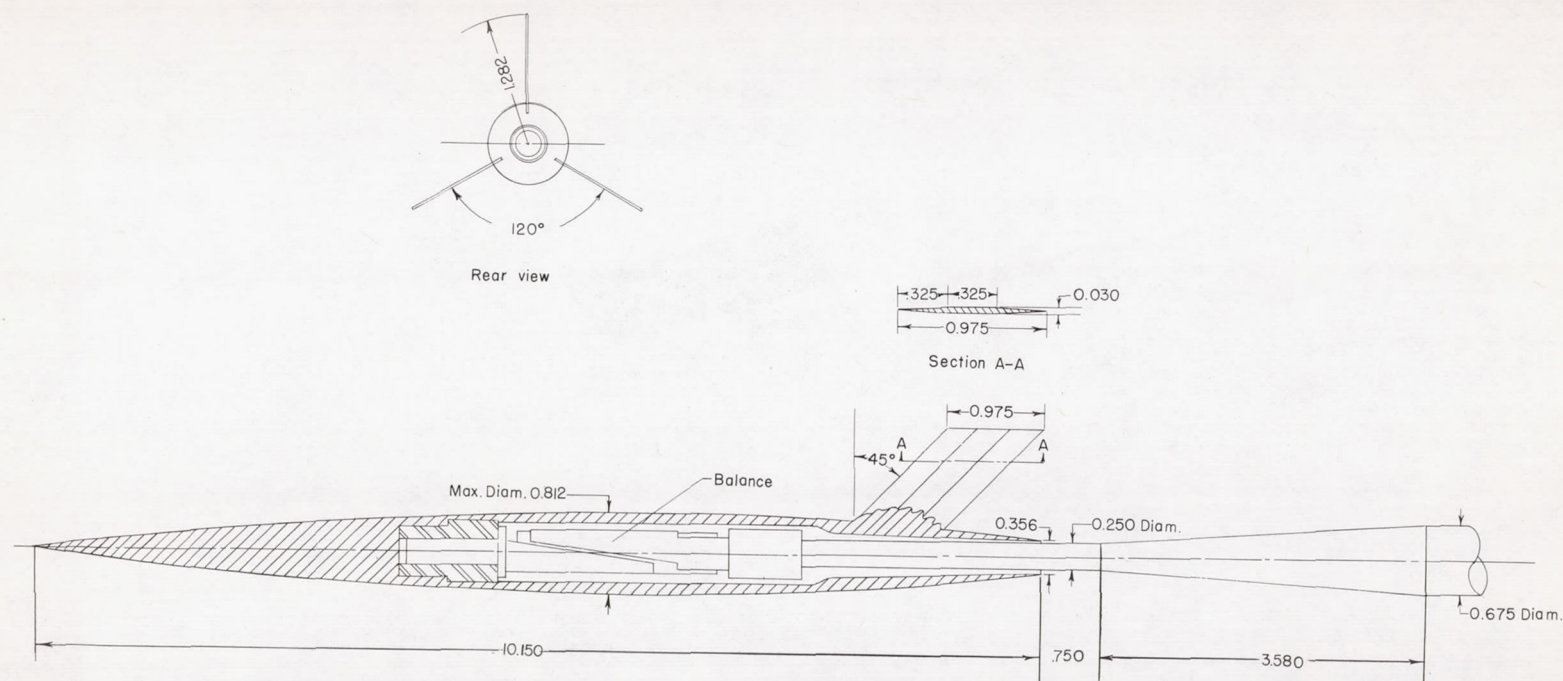
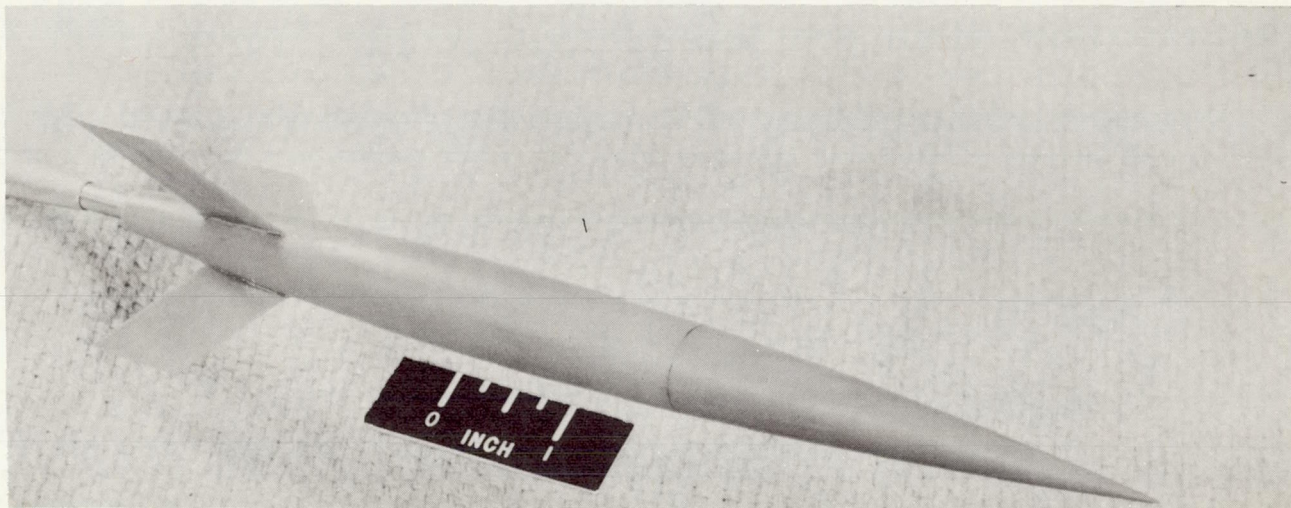
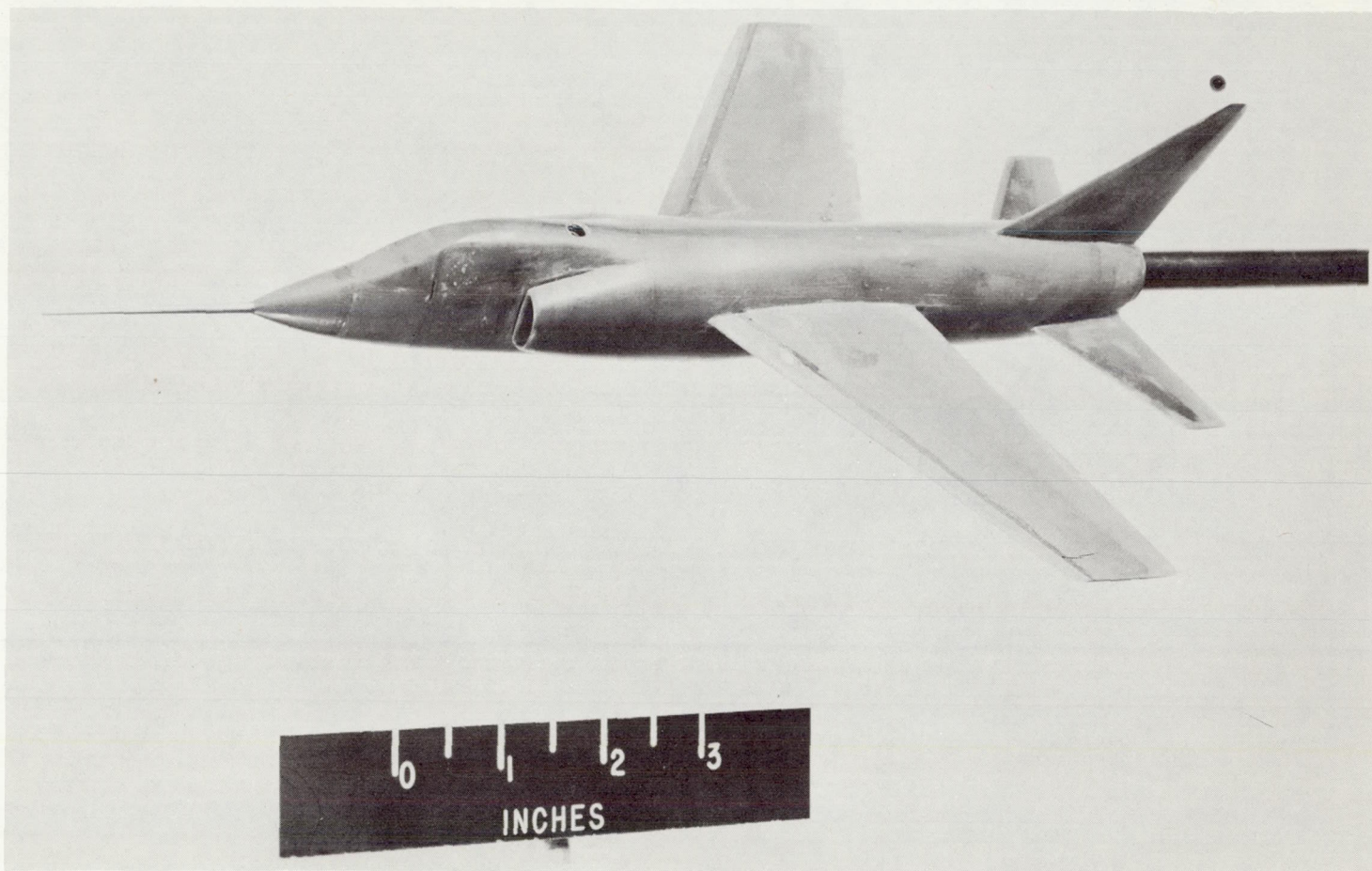


Figure 1.- Diagrammatic sketch showing model as mounted in wind tunnel. All dimensions are in inches.



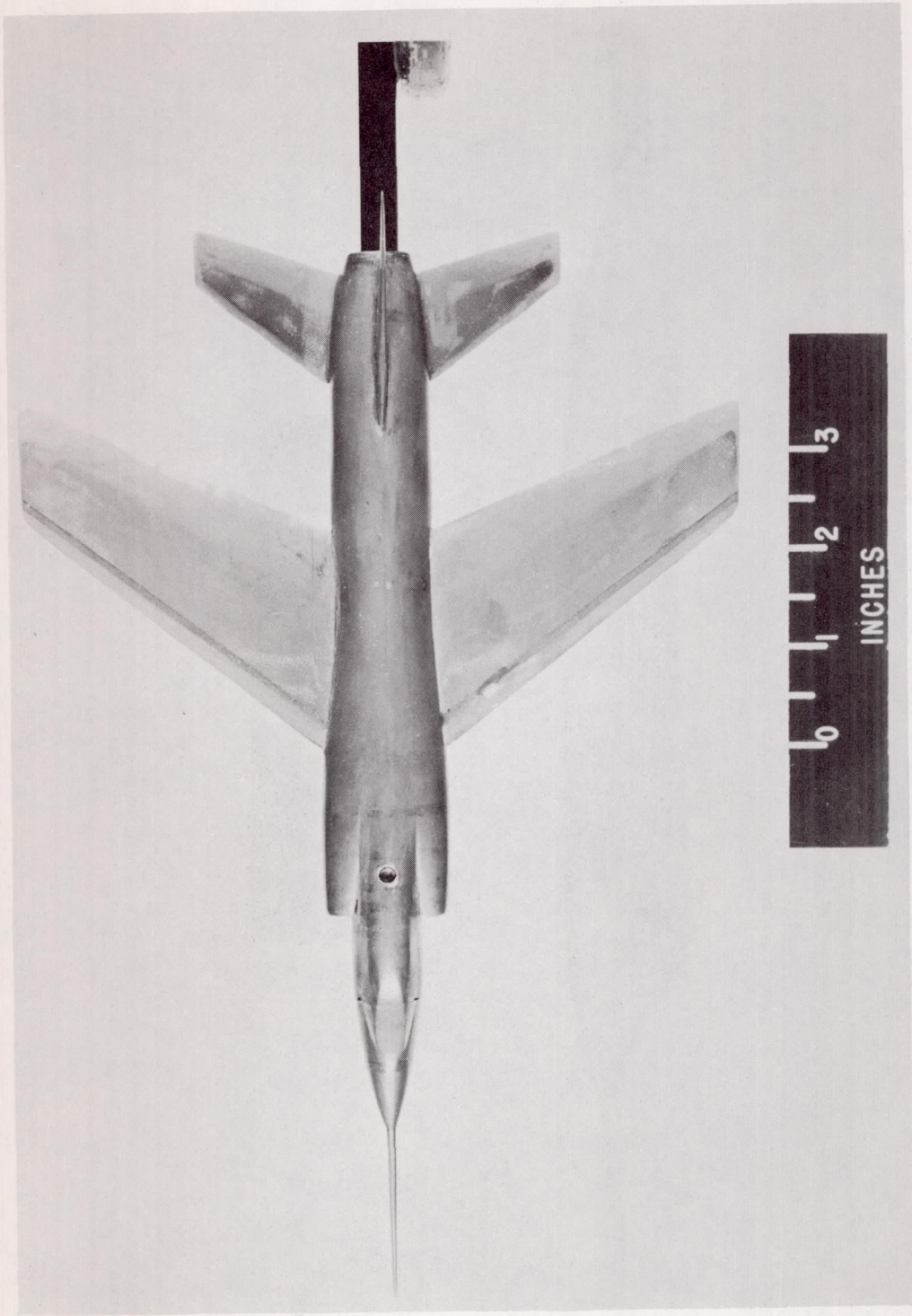
L-86628.1

Figure 2.- Photograph of the fin-stabilized model.



(a) Three-quarter view from above. L-94640

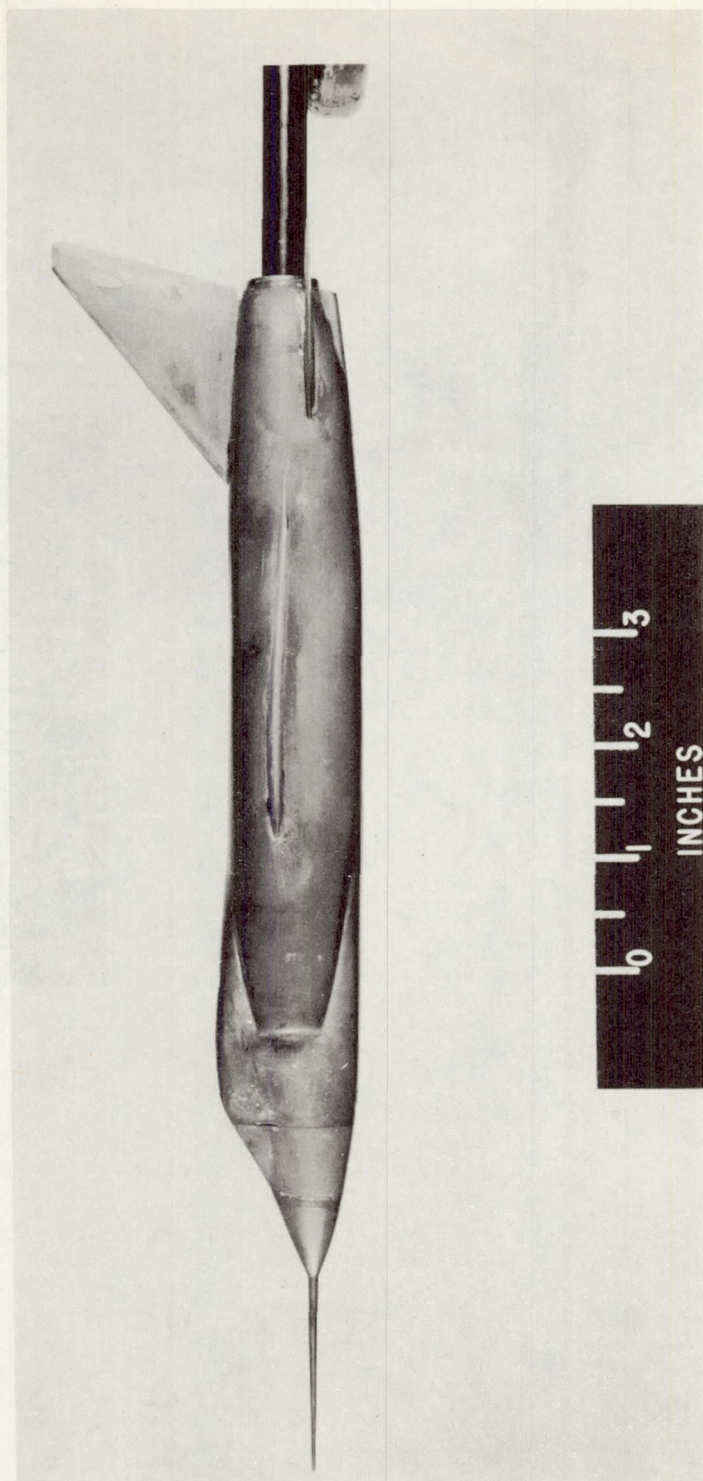
Figure 4.- Photographs of airplane model.



L-94639

(b) Plan view.

Figure 4.- Continued.



L-94638

(c) Side view.

Figure 4.- Concluded.

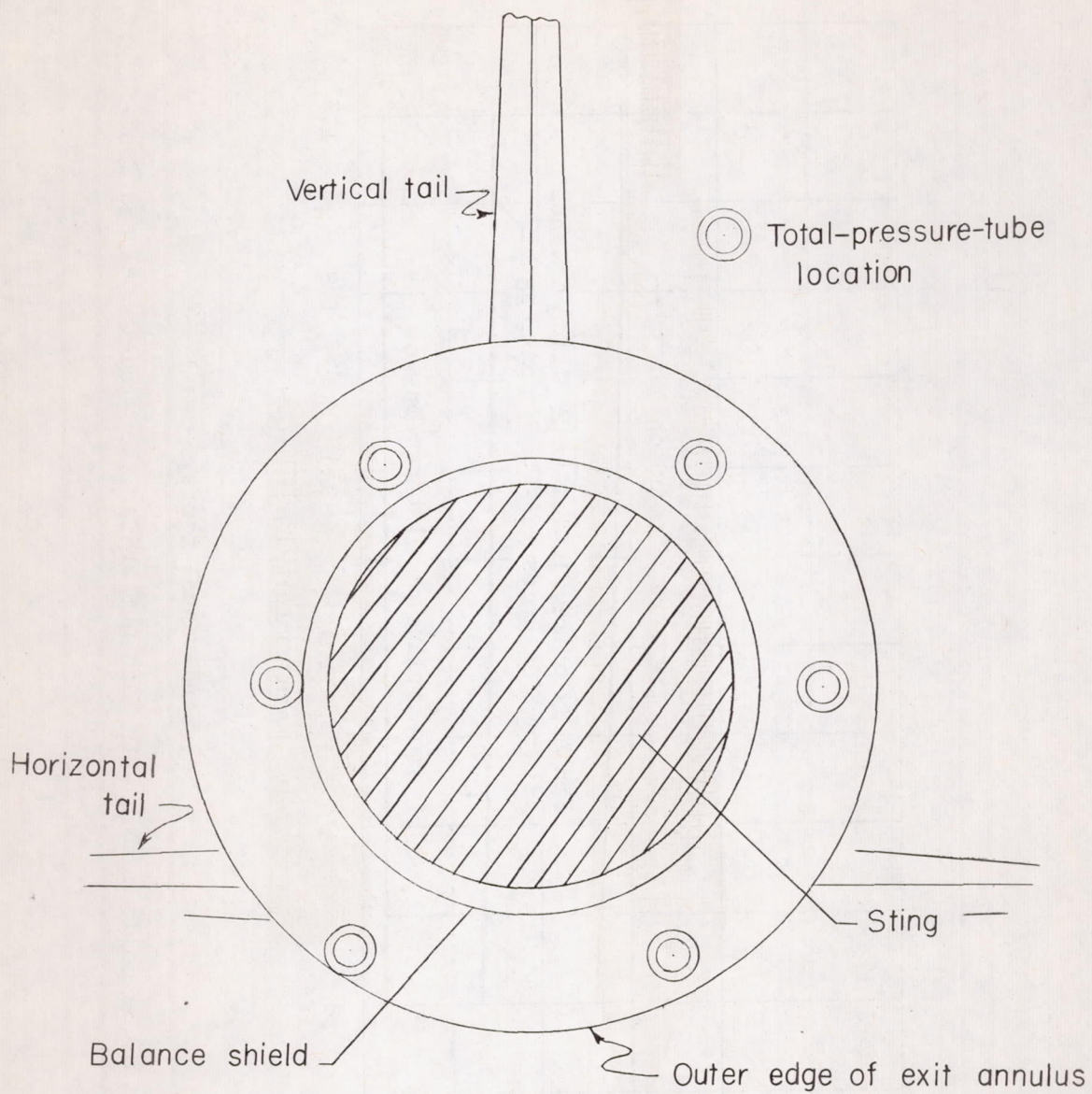
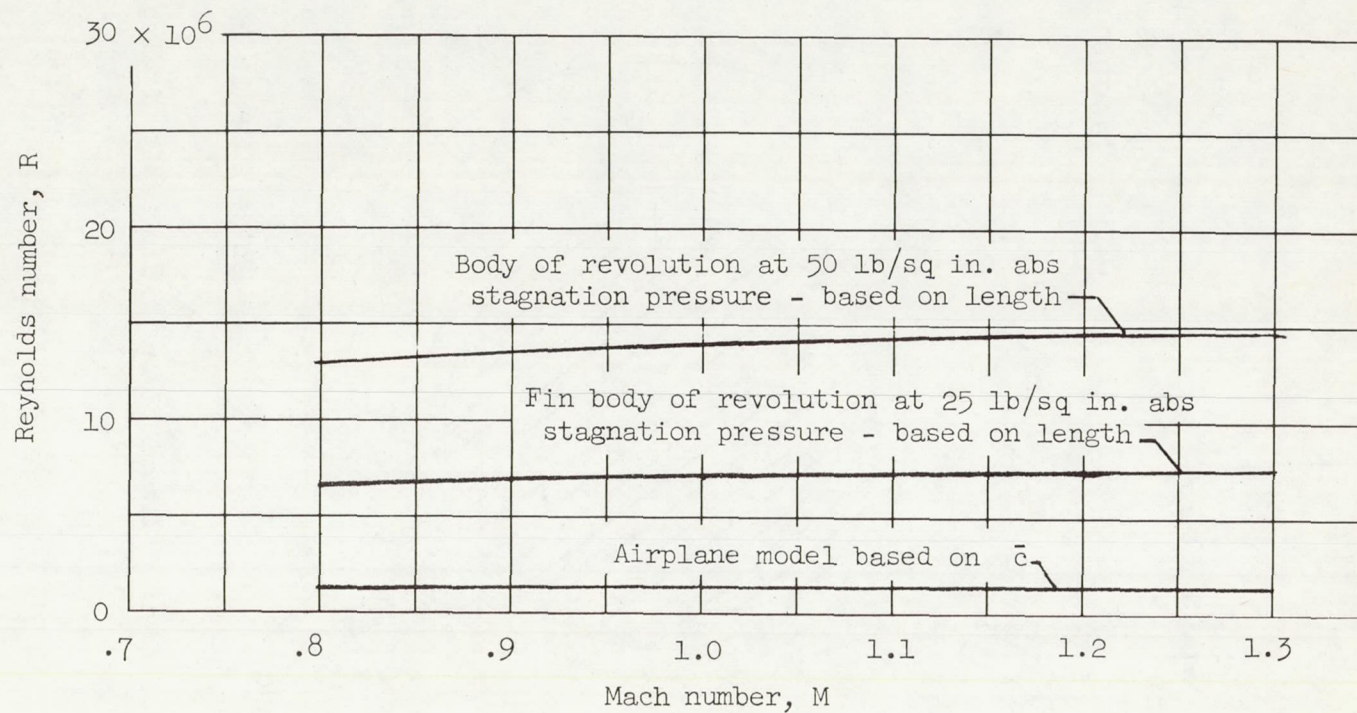
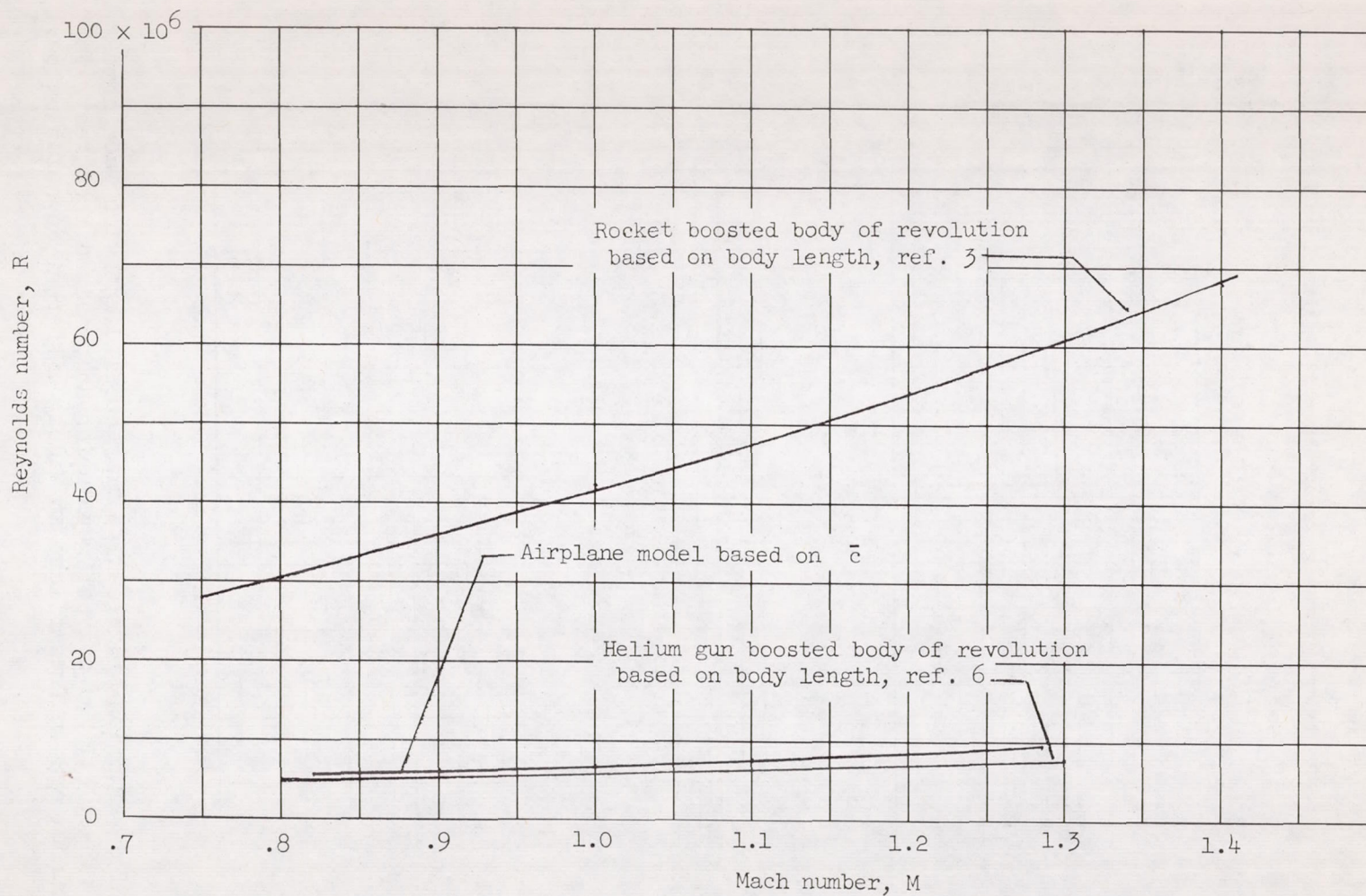


Figure 5.- Total-pressure-tube distribution at flow exit of airplane model.



(a) Wind-tunnel tests.

Figure 6.- Variation of Reynolds number with Mach number for the wind-tunnel and free-flight tests.



(b) Free-flight tests.

Figure 6.- Concluded.

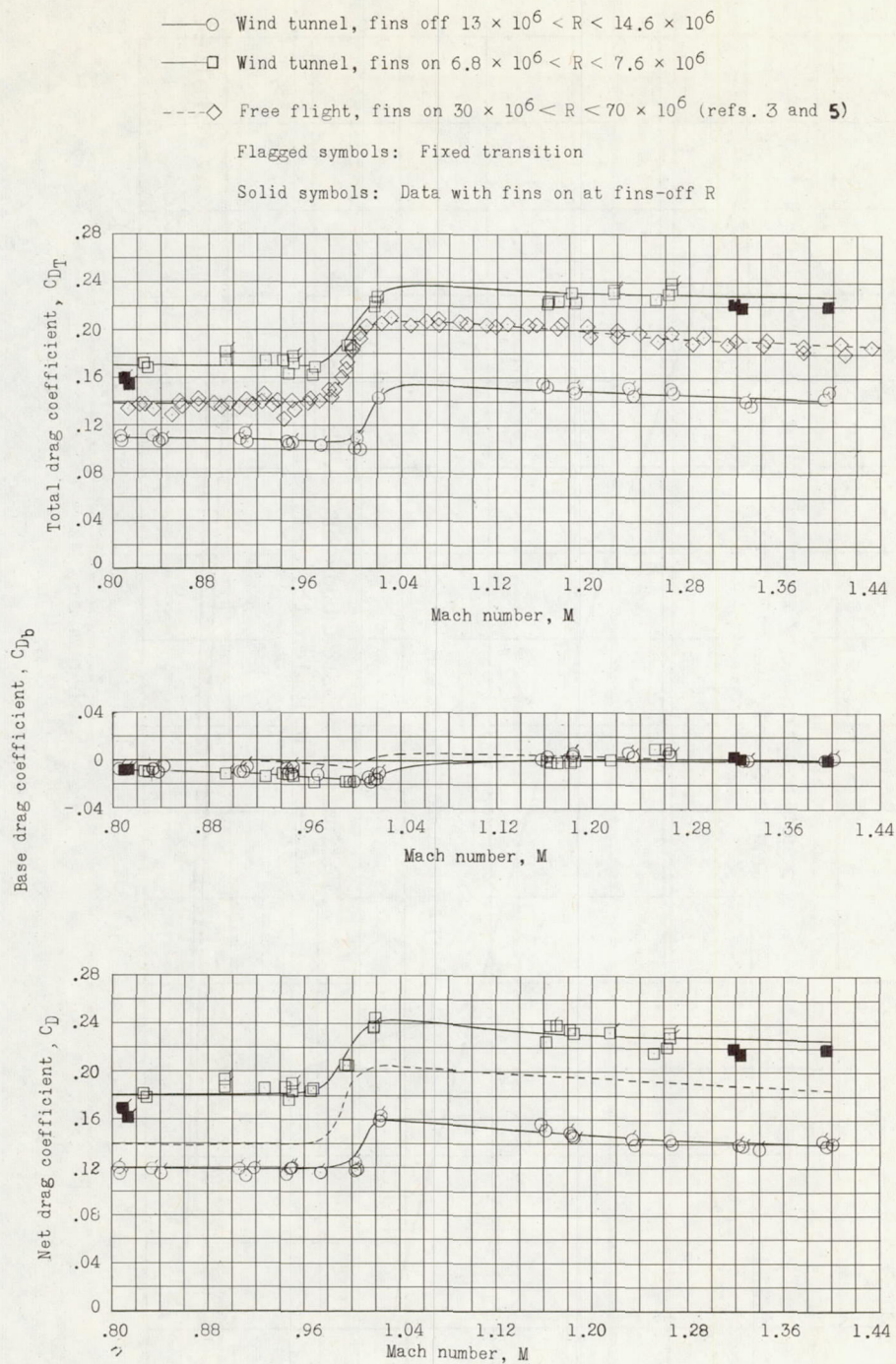


Figure 7.- The variation of zero-lift drag coefficient with Mach number for the fin-stabilized body of revolution as obtained from tests in a wind tunnel and in free flight at widely different Reynolds number.

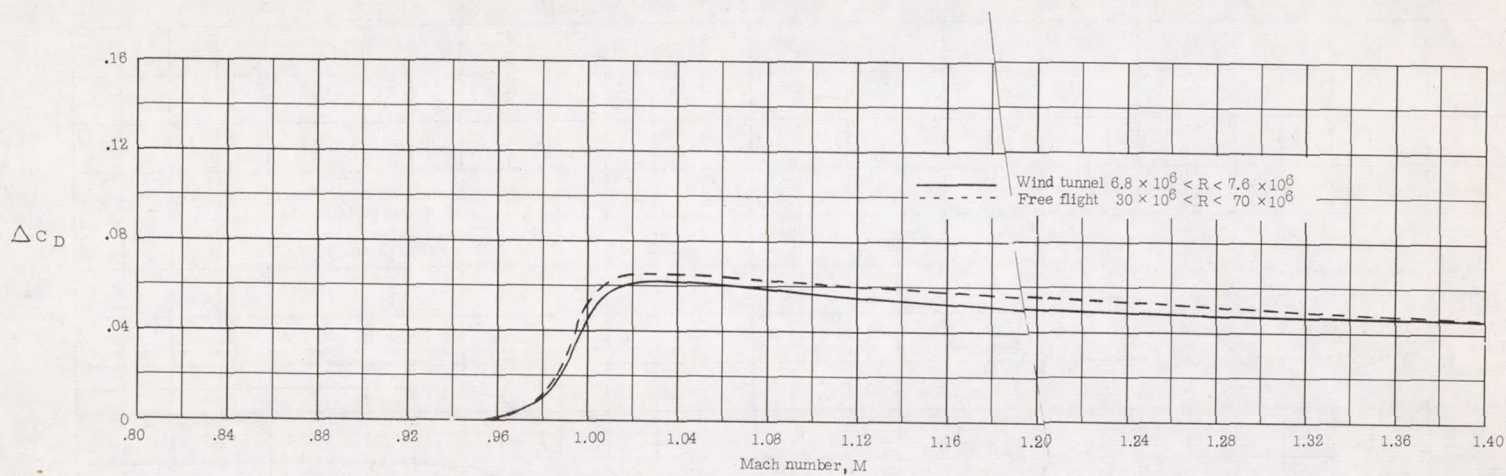


Figure 8.- Comparison of variation of pressure-drag coefficient rise with Mach number as obtained from wind-tunnel and free-flight tests of a fin-stabilized body of revolution.

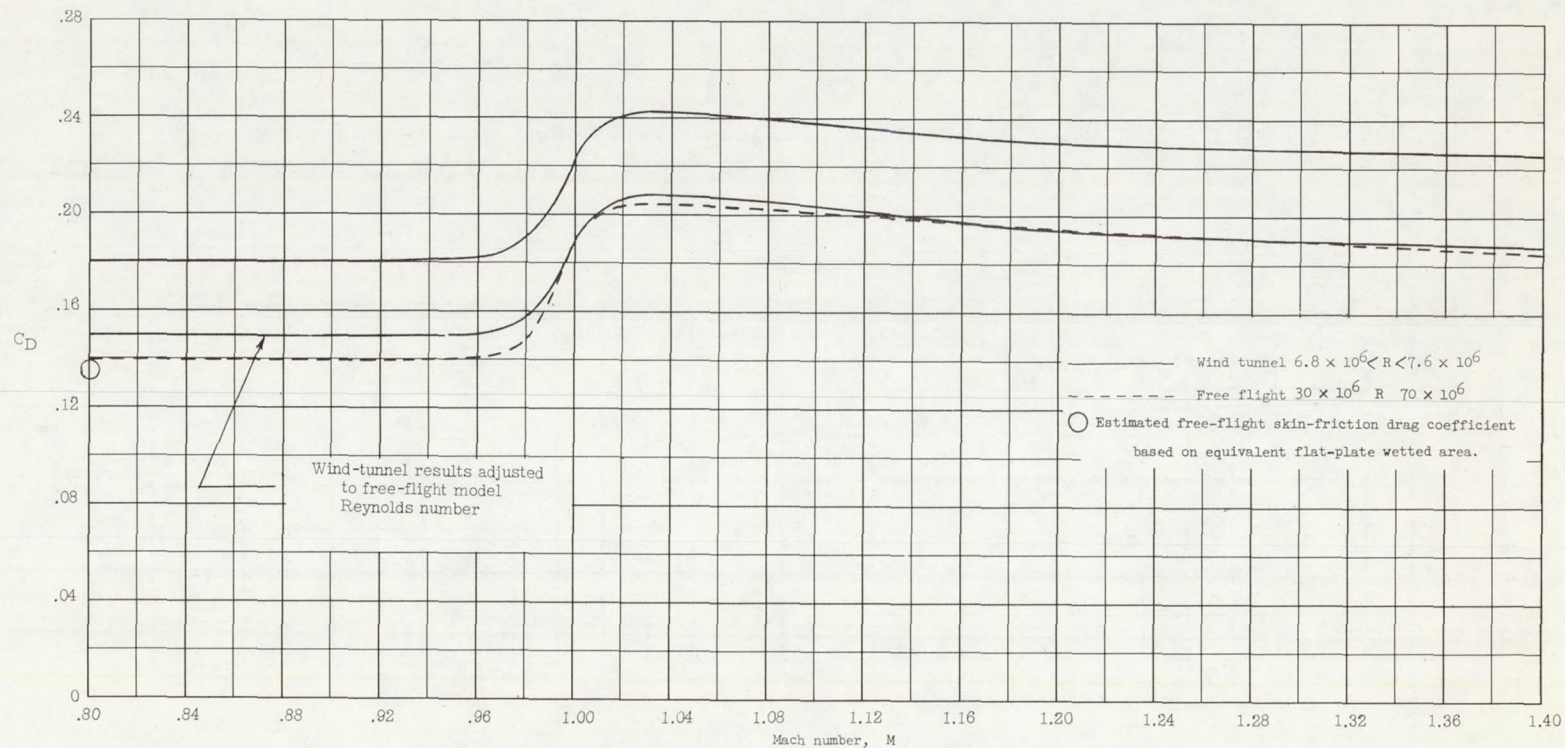


Figure 9.- Comparison of net drag coefficient for the fin-stabilized body of revolution as obtained at widely different Reynolds numbers.

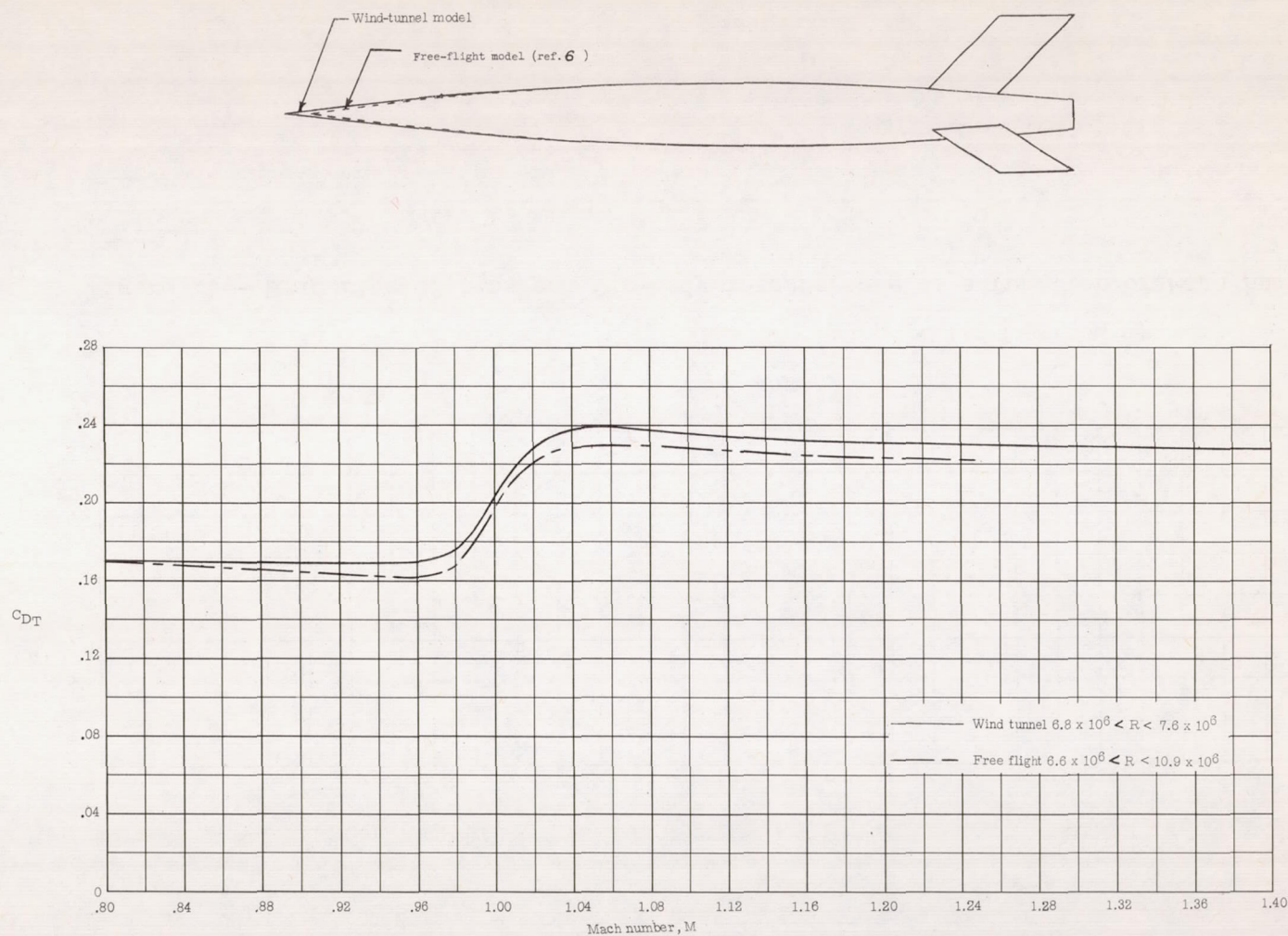


Figure 10.- Comparison of total drag coefficient as obtained from wind-tunnel and free-flight tests of similar models at approximately the same Reynolds number. Data unadjusted for base-pressure differences.

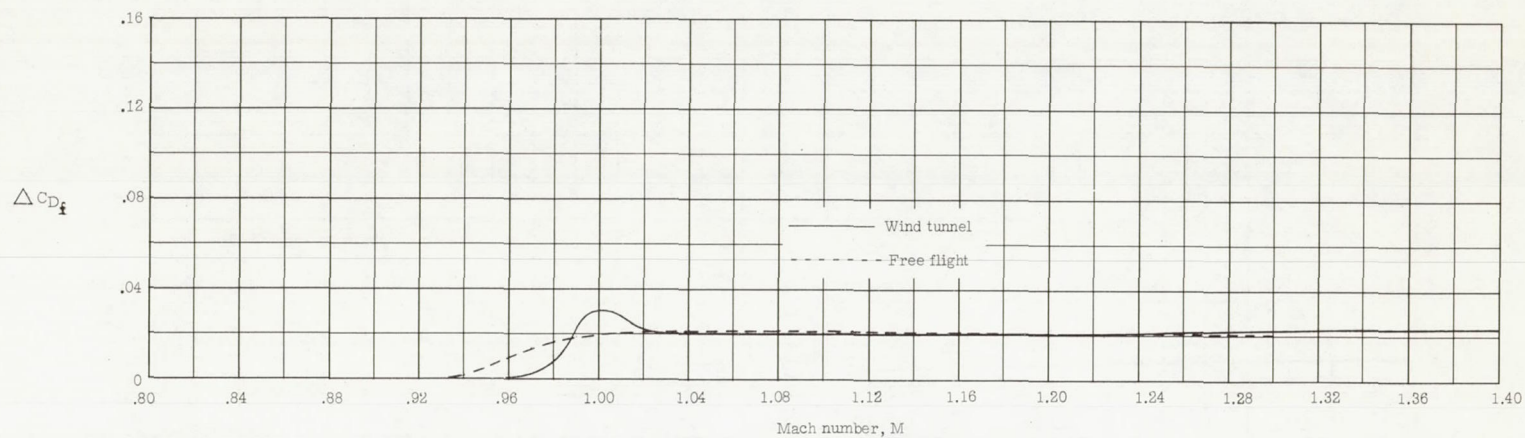


Figure 11.- Drag rise of fins and fin-body interference as a function of Mach number.

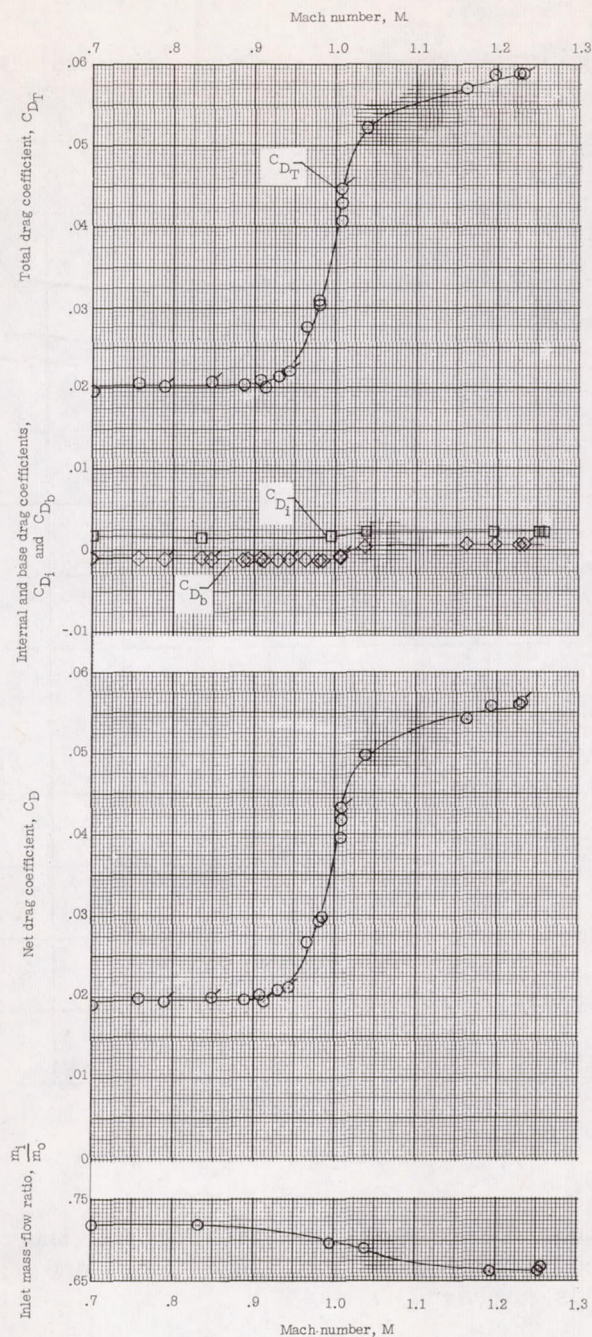


Figure 12.- The variation of zero lift-drag coefficient and the inlet mass-flow ratio with Mach number for the airplane configuration tested in the wind tunnel. Reynolds number $\approx 1.2 \times 10^6$; flagged points are check points.

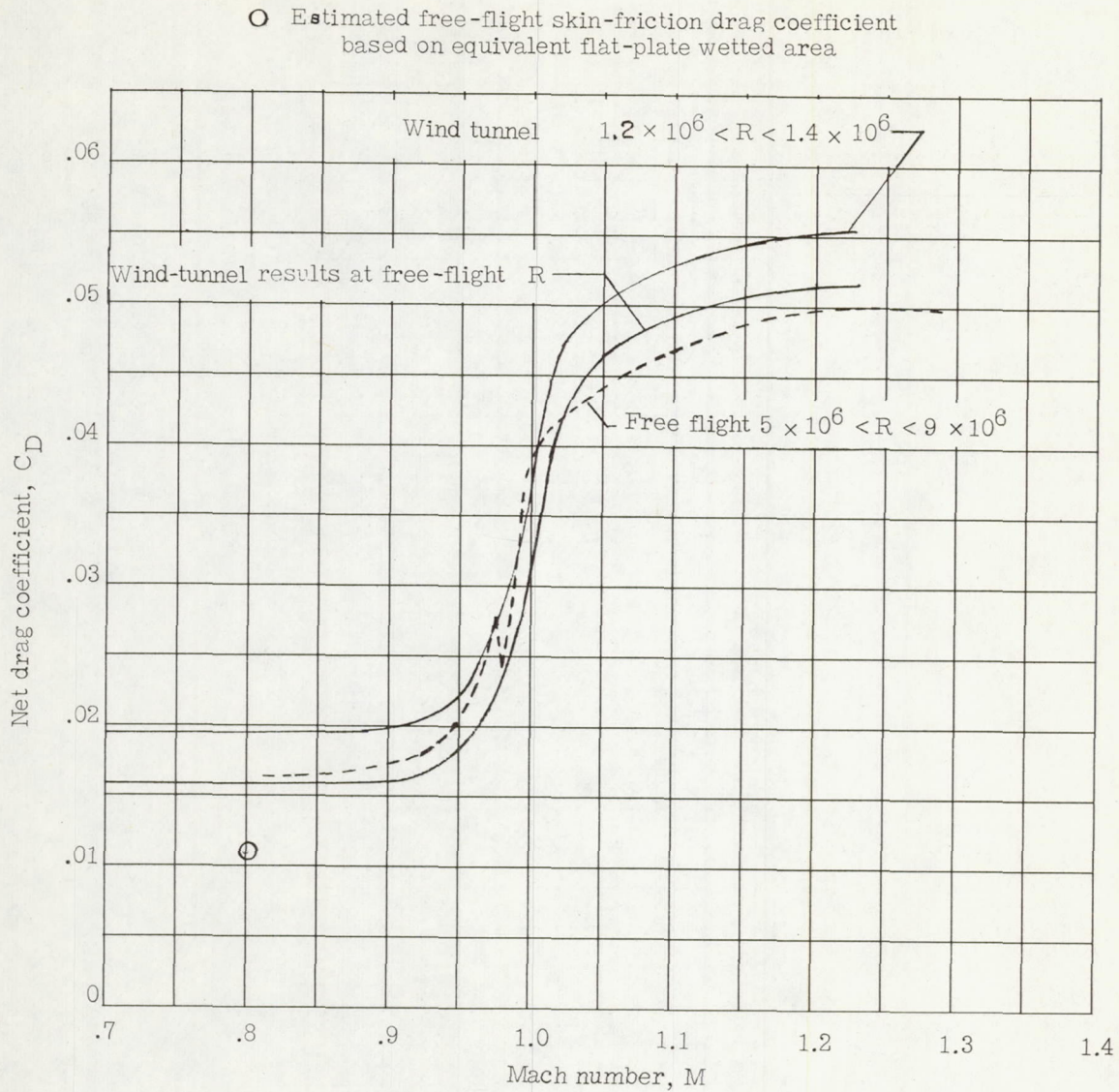


Figure 13.- Comparison of net drag coefficient for the airplane configuration as obtained from tests in a wind tunnel and free flight at different Reynolds numbers.